



# Formation of Anionic C, N-bearing Chains in the Interstellar Medium via Reactions of $H^-$ with $HC_xN$ for Odd-valued $x$ from 1 to 7

F. A. Gianturco<sup>1</sup> , M. Satta<sup>2</sup>, E. Yurtsever<sup>3</sup>, and R. Wester<sup>1</sup>

<sup>1</sup>Institut für Ionenphysik und Angewandte Physik Universität Innsbruck, Technikerstr. 25/3, A-6020 Innsbruck, Austria; [Francesco.Gianturco@uibk.ac.at](mailto:Francesco.Gianturco@uibk.ac.at)

<sup>2</sup>CNR-ISMN and Department of Chemistry, The University of Rome Sapienza, P.le A. Moro 5, I-00185 Rome, Italy

<sup>3</sup>Department of Chemistry, Koç University, Rumelifeneriyolu, Sariyer, TR-34450, Istanbul, Turkey

Received 2017 June 12; revised 2017 September 13; accepted 2017 October 9; published 2017 November 15

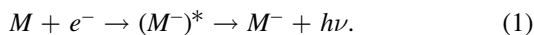
## Abstract

We investigate the relative efficiencies of low-temperature chemical reactions in the interstellar medium with  $H^-$  anion reacting in the gas phase with cyanopolyynes neutral molecules, leading to the formation of anionic  $C_xN^-$  linear chains of different lengths and of  $H_2$ . All the reactions turn out to be without barriers, highly exothermic reactions that provide a chemical route to the formation of anionic chains of the same length. Some of the anions have been observed in the dark molecular clouds and in the diffuse interstellar envelopes. Quantum calculations are carried out for the corresponding reactive potential energy surfaces for all the odd-numbered members of the series ( $x = 1, 3, 5, 7$ ). We employ the minimum energy paths to obtain the relevant transition state configurations and use the latter within the variational transition state model to obtain the chemical rates. The present results indicate that at typical temperatures around 100 K, a set of significantly larger rate values exists for  $x = 3$  and  $x = 5$ , while the rate values are smaller for  $CN^-$  and  $C_7N^-$ . At those temperatures, however, all the rates turn out to be larger than the estimates in the current literature for the radiative electron attachment (REA) rates, thus indicating the greater importance of the present chemical path with respect to REA processes at those temperatures. The physical reasons for our findings are discussed in detail and linked with the existing observational findings.

*Key words:* astrochemistry – ISM: clouds – ISM: molecules – ISM: planetary nebulae – molecular processes

## 1. Introduction

The possibility that molecular systems formed as stable species with a negative charge (anionic molecules) and to have them exist in detectable amounts in the interstellar medium (ISM), more specifically in cold dark clouds environments, was put forward several years ago by various authors (Dalgarno 1973; Sarre 1980; Herbst 1981; Herbst & Woon 1997). They further suggested that carbon chains and hydrocarbon radicals would have large and positive electron affinities (EA) and could therefore be more likely to lead to anion formations via the energy-releasing mechanism of radiative electron attachment (REA). The latter process would occur from the interactions of such molecules with the free electrons generated in the diffuse regions by H and He photoionization. The recombination process would then be



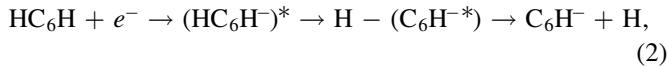
They further surmised that the above processes would provide efficient mechanisms for stabilizing molecular anions when the initial neutrals were made up of more than four or five atoms (Herbst & Osamura 2009). The experimental astrochemical evidence for the presence of such species was only provided later on, when an unidentified series of lines was detected in a radio astronomical survey of the evolved carbon star IRC+10216 by Kawaguchi et al. (1995), and was conclusively assigned to the spectrum of  $C_6H^-$  by McCarthy et al. (2006) on the basis of laboratory rotational spectroscopy and separate observations toward the Taurus Molecular Clouds I (TMC-I(CP)). Additional anionic molecules were observed later on by Cernicharo et al. (2007) ( $C_4H^-$ ), by Remijan et al. (2007) ( $C_8H^-$ ) and by Thaddeus et al. (2008) ( $C_3N^-$ ) in the envelope of IRC+10216. In TMC-I the  $C_8H^-$  anions was additionally observed by Brunken et al. (2007), the largest

anionic molecular chain observed thus far. Additional observations of molecular negative ions were surveyed by Gupta et al. (2007), who observed  $C_6H^-$  in two further sources: the prestellar cloud L1544 and the protostellar object L1521F.

Since polyatomic molecules with a negative charge have turned out to be present under different conditions and in significant quantities (e.g., the measured column density of  $C_6H^-$  in TMC-I(CP) was found by McCarthy et al. (2006) to be  $10^{11} \text{ cm}^{-2}$ ), it is reasonable to expect that they also play a significant role in the chemistry of the dark molecular clouds and at the low temperatures assigned to these regions. Hence, it becomes relevant to investigate in more detail additional possible formation paths of such stable anionic species by chemical routes.

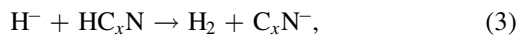
Although for different molecular partners, in recent years we have already studied the general dynamics that could be driven by the free electrons available in that environment, and the important role played by intermediate, metastable anions as molecular gateways to the final, anionic species, which are experimentally detected. For example, the resonant attachment of slow electrons to  $NCCN$  was studied a while ago (Sebastianelli & Gianturco 2010), and we also analyzed the possible fragmentation decays of  $HC_3N$  and  $HC_5N$  upon electron attachment (Sebastianelli & Gianturco 2012), as well as carried out a detailed study of resonant electron attachment to  $HC_4H$  (Baccarelli et al. 2013). A more extensive analysis on the dynamics of electron attachment to non-polar hydrocarbon chains like  $HC_nH$  (with  $n$  from 4 to 12) at the expected low energies of planetary atmospheres and dark molecular clouds, was also carried out (Carelli et al. 2013). In that work it was specifically shown that the attachment mechanism is driven by the prior formation of metastable anions from asymmetrically deformed non-polar polyynes, giving rise to complex intermediates of polar radical anions plus H-atom-stretched

configurations:



where the intermediate system can initially form its closed-shell anion as a dipole-bound state partner. The latter can then decay into the more stable anionic valence-bound states, after internal-energy redistribution and ejection of one terminal hydrogen atom. The above chain of events is reminiscent of the indirect REA mechanism (IREA) introduced more recently by Douguet et al. (2013), where the dissipation paths of the large amount of energy that has to be released upon electron attachment in systems with large and positive EA values was suggested to occur via an electron-vibration nonadiabatic coupling mechanism. They have shown, however, that this IREA mechanism, and indeed also the REA mechanism of Equation (1), are unfortunately rather inefficient for the smaller radical chains like  $\text{C}_2\text{H}^-$  and  $\text{C}_4\text{H}^-$ , thereby calling into question the relevance of such pathways for the formation of observable quantities of the anions of the present molecules. It is therefore important to further explore and understand which other mechanisms could be responsible for the formation of the smaller (C, N)-chains anions under ISM conditions.

To extend the chemical formation option, we wish to explore in the present study a “chemical” stabilization of the anions that involve four of the members of the C-bearing linear chains that terminate with the cyano group (Morisawa et al. 2005). We shall therefore look at the efficiency of the formation of such anions by examining the reaction of  $\text{H}^-$  with non-polar precursors of the cyanopolyne series, the  $(\text{HC}_x\text{N})$  molecules, in the gas phase:



where the length of the odd-numbered chains goes in our study from  $x = 1$  to  $x = 7$ .

The importance of  $\text{H}^-$  as a chemical partner has been suggested before, given its likely existence through cosmic rays, which act during the ion-pair reactions within the inner cores (radius  $\leq 10^6$  au) of the prestellar envelopes (Prasad & Huntress 1980), although little is known, so far, about the details of its actual mechanism under the above conditions (Mackay et al. 1977).

Therefore, if the presence of  $\text{H}^-$  could be in sufficient amounts to provide a useful chemical partner, then we shall show that the above reaction is indeed an interesting alternative. They are in fact, as discussed below, markedly exothermic processes where the final product formations involve an electron transfer (ET) mechanism accompanied by the formation of a new  $\text{H}_2$  bond into a separate molecular product from the final anion.

In an earlier study on the smaller members of the cyanoderivatives,  $\text{CN}^-$  and  $\text{C}_3\text{N}^-$  (Satta et al. 2015), we indicated that the chemical nature of their reactions with  $\text{H}^-$ , i.e., the suggested mechanism of an ET process occurring along with the energy release from the  $\text{H}_2$  formation, makes the production of their anions exothermic and occurs without an intermediate energy barrier between reactants and products, although a configurational transition state (TS) is observed. It thus becomes interesting to computationally extend the study of these reactions to verify their behavior for larger members of the series, as well as revisit the earlier results using an

improved description of the quantum chemical interaction forces.

In the following sections we shall investigate this point for the reactions involving the first four members of the cyanopolyne series. In Section 3 we analyze the overall shapes of the various RPESs, while in Section 4 we calculate the corresponding reaction rates over a range of temperatures representing the colder dark cloud conditions and the warmer circumstellar envelopes that are of interest in our study. In Section 5 we give our present conclusions and also link them with the existing observational studies on the abundances of the cyanopolyne anions.

## 2. Quantum Chemical Calculations

Before starting our analysis of the dynamical features of the reactive partners in Equation (3), we need to look into the quantum structural properties that we have obtained for all the partners in the considered processes. All the ab initio structural calculations were carried out using the MOLPRO suite of codes (Werner et al. 2006), unless otherwise stated. In order to better analyze visible trends along the present series of linear anions, we have repeated the calculations for the smaller terms of the series, the  $x = 1$  and the  $x = 3$  molecular anions already investigated before (Satta et al. 2015). We have also extended the analysis of the kinetics of  $\text{CN}^-$  formation by considering both isomeric structures of the initial molecule, HCN and HNC. More details on this aspect of the discussion will be given below.

The method employed here has been the Coupled-Cluster-Single-Double-Perturbative-Triple-Excitation (CCSD(T)) method and the quality of the chosen basis sets is defined as augmented-correlation-consistent, corrected up to triple-zeta expansions: aug-cc-p-VTZ. All the present acronyms are explained in detail in the MOLPRO suite of codes (Werner et al. 2006). All the molecular reagents, as already known, turned out to be linear in the most stable ground electronic states that correspond to closed-shell structures. Their optimized geometries are presented in Table 1. We also report in that table the geometries of the isomer radicals  $\text{C}_x\text{NH}$  so that they can be compared with the corresponding structures of the  $\text{HC}_x\text{N}$  species.

One clearly sees from the table’s data that only minor differences in the geometries occur when going from the  $\text{HC}_x\text{N}$  to  $\text{C}_x\text{HN}$ ; we shall further analyze the possible effects on the energy changes of these exothermic reactions. The total energies for the ground states of reagents and products are reported in Table 2

As mentioned earlier, all the present reactions are exothermic processes involving polar targets. To check on the quality of our description of them, we report in Table 3 the calculated values of the permanent dipoles of the molecular partners undergoing the ET process during the reactions.

Note that the dipole moment of the CN radical is found, ensuing the largest basis set in the bottom line in the table, to vary between  $-1.379$  and the CCSD(T) approach (last column to the right) of  $-2.307$  Debye. An older experimental value is  $1.45$  (Thomson & Dalby 1968) while a recent calculation by Fortenberry & Crawford (2011) yielded a value of  $-1.47$ .

For  $\text{C}_3\text{N}$ ,  $\text{C}_5\text{N}$ , and  $\text{C}_7\text{N}$  the largest basis set was used within the density functional approach (DFT) using the B3LYP exchange functional model, providing decreasing values of  $-2.95$ ,  $+0.80$ , and  $+1.30$  from Debye in Table 3. Our earlier calculations yielded values of  $-3.0$ ,  $+0.80$ , and  $1.29$ : no

**Table 1**  
Computed, Optimized Geometries for the Neutral Radicals and Negative  $^1\Sigma$  Molecules of the Present Study

$C_xN^-$	$x = 1$	$x = 3$	$x = 5$	$x = 7$
C1C2	...	1.263	1.271	1.275
C2C3	...	1.364	1.342	1.333
C3C4	...	...	1.246	1.255
C4C5	...	...	1.352	1.329
C5C6	...	...	...	1.247
C6C7	...	...	...	1.351
C(last)N	1.191	1.187	1.188	1.188
$HC_xN$	$x = 1$	$x = 3$	$x = 5$	$x = 7$
C1C2	...	1.217	1.222	1.224
C2C3	...	1.372	1.359	1.354
C3C4	...	...	1.228	1.235
C4C5	...	...	1.364	1.347
C5C6	...	...	...	1.233
C6C7	...	...	...	1.361
C(last)N	1.167	1.177	1.180	1.181
C1H	1.065	1.063	1.064	1.063
$C_xNH$	$x = 1$	$x = 3$	$x = 5$	$x = 7$
C1C2	...	1.274	1.284	1.289
C2C3	...	1.313	1.305	1.303
C3C4	...	...	1.263	1.271
C4C5	...	...	1.300	1.292
C5C6	...	...	...	1.269
C6C7	...	...	...	1.298
C(last)N	1.177	1.178	1.184	1.187
NH	0.998	0.995	0.996	0.996

**Note.** All species are linear and the distances are in Å.

**Table 2**  
Computed Ground State Total Energies for Reactants, Using the CCSD(T) Method Described in the Main Text

Molecule	aug-cc-pVTZ energy
H <sub>2</sub>	-1.172613
H <sup>-</sup>	-0.526562
C <sub>3</sub> N <sup>-</sup>	-168.723503
C <sub>5</sub> N <sup>-</sup>	-244.743867
C <sub>7</sub> N <sup>-</sup>	-320.762897
HC <sub>3</sub> N	-169.288765
HC <sub>7</sub> N	-245.302425
HC <sub>7</sub> N	-321.317307

**Note.** All values are in units of hartrees.

experimental values or earlier calculations exist on the radicals, as discussed by Carelli et al. (2014). On the other hand, all the corresponding anions have very different dipole moment values, as reported in the last columns of Table 3 and as computed earlier by Carelli et al. (2014); no experimental values are available for the closed-shell anions, while earlier calculations by Botschwina & Oswald (2008) and by Kolos et al. (2008) yielded dipole moment values with the same orientation (i.e., along the  $z$ -axis and now pointing from the N to the C atoms in each member of the series) and about 20% larger.

**Table 3**  
Computed Permanent Dipole Moments (in Units of Debye) for the Neutral Counterparts of the Final Product. (RODFT, ROMP2 and ROCCSD(T) Denote Restricted-open-shell Calculations)

	RODFT (B3LYP)	ROMP2	ROCCSD(T)	Anion <sup>a</sup>
CN	...	...	...	...
6-311G(2df, 2pd)	-1.3058	-2.2765	-2.2569	0.69
6-311++G (3df, 3pd)	-1.3811	-2.3256	-2.3087	...
cc-pVTZ	-1.3222	-2.2847	-2.2672	...
aug-cc-pVTZ	-1.3794	-2.3233	-2.3069	...
C <sub>3</sub> N	...	...	...	Anion <sup>a</sup>
6-311G(2df, 2pd)	-2.8394	-3.1759	-3.1753	2.72
6-311++G(3df, 3pd)	-2.9571	-3.2539	-3.2533	...
cc-pVTZ	-2.8807	-3.2058	-3.2052	...
aug-cc-pVTZ	-2.9552	-3.3252	-3.2506	...
cc-pVQZ	-2.9340	...	...	...
aug-cc-pVQZ	-2.9554	...	...	...
C <sub>5</sub> N	...	...	...	Anion <sup>a</sup>
6-311G(2df, 2pd)	1.2490	-0.3117	...	5.61
6-311++G(3df, 3pd)	1.2796	-0.3310	...	...
cc-pVTZ	1.2997	-0.2992	...	...
aug-cc-pVTZ	1.2932	-0.3181	...	...
C <sub>7</sub> N	...	...	...	Anion <sup>a</sup>
6-311G(2df, 2pd)	0.7796	-0.4389	-0.4389	4.19
6-311++G(3df, 3pd)	0.7888	-0.4648	...	...
cc-pVTZ	0.8083	-0.4352	-0.4352	...
aug-cc-pVTZ	0.7978	-0.4541	...	...

**Note.**

<sup>a</sup> Anion values are from Carelli et al. (2014).

**Table 4**  
Computed EA Values at the CCSD(T) Level of Calculation of the Present Study (eV)

	Present Calculations	Expt(Carelli et al. 2014)	Calculations(Carelli et al. 2014)
CN	4.00	3.86	3.80
C <sub>3</sub> N	4.64	4.59	4.40
C <sub>5</sub> N	5.09	...	4.59
C <sub>7</sub> N	5.51	...	4.61

In all cases, therefore, the dipole moment values increase dramatically in going from the radical to the closed-shell anionic structures. Along the same series of cyanopolynes, the corresponding electron affinities (EA) also increase rather markedly from the  $n = 1$  member (+3.8 eV) to the  $n = 7$  member (+4.61 eV), as discussed already in Carelli et al. (2014). This means that the occurrence of the ET step during the reactions we are going to discuss affords large energy releases when the electron moves from the H<sup>-</sup> partner (with an EA value of 0.754 eV Shiell et al. 2000) to the N-end of the final linear chains with much larger EA values. This aspect will be discussed in more detail below.

We have again computed the EA values at the equilibrium geometries of the present radicals and found the results reported below in Table 4.

We can see from the table that all the present radicals have very large EA values, thus making the ET process from the H<sup>-</sup>

**Table 5**

Computed Exothermicity Values for the Two Series of Reactions Involving Both Isotopologue Forms (Units Are in eV)

$H^- + HC_xN \rightarrow H_2 + C_xN^-$			
x	MP2	MP2+ZPE	CCSD(T)
1	2.11	2.14	2.12
3	2.17	2.19	2.20
5	2.37	2.40	2.38
7	2.53	2.58	2.49
$H^- + HNC_x \rightarrow H_2 + NC_x^-$			
x	MP2	MP2+ZPE	CCSD(T)
1	2.89	2.90	2.76
3	4.59	4.56	4.48
5	5.19	5.17	5.14
7	5.54	5.55	

reagent into the final anions a strongly exothermic process leading to the TS formation complex before the additional energy release due to the formation of the neutral  $H_2$  bond during formation of the final molecular products. Below, we shall illustrate in more detail the energetics of the present reactions.

If we look at the data at the CCSD(T) level of calculations, we see that all the reactions involving the  $HC_xN$  reagents are consistently exothermic along the series, varying by more than 10% as  $x$  increases from 1 to 7; as we shall further see below, none of them show any barrier from reagents to products, thus confirming their feasibility at the low temperatures of the DMC environments.

Additionally, we see that the same set of reactions, involving their isotopologue variants, occurs with the  $HNC_x$  series of reagents (lower panel in Table 5).

The exothermicity values increase quite markedly: an increase of about 0.64 eV for the HCN/HNC case, to more than 2.60 eV for the  $HNC_7$  case. This is an interesting result for which, however, we have little observational information for the members with  $x$  from 3 to 7. On the other hand, the HCN/HNC isotopologues have been extensively observed in many astrophysical environments, from diffuse and translucent interstellar clouds in Listz & Lucas (2001) and Turner et al. (1997); to dense interstellar clouds in Mily-Blant et al. (2010); to star-forming regions in Jin et al. (2015); to protoplanetary disks in Graninger et al. (2015); to external galaxies in Gao et al. (2004); as well as comets in Lis et al. (2008); and planetary atmospheres in Moreno et al. (2011).

Likewise, the HCN/HNC abundance ratios have also shown marked changes between different astrochemical environments. In the dense interstellar clouds, in fact, the gas is shielded from external UV starlight and the abundance ratio was found to be around 1.0 in Sarrasin et al. (2010). On the other hand, in regions exposed to UV photons, HCN was found to be more abundant than HNC by a factor of 5 in both diffuse clouds (Listz & Lucas 2001) and in PDR environments (Hogerheijde et al. 1995). It therefore stands to reason that both reactions could occur with  $H^-$ , thereby increasing the probability of forming  $CN^-$ , as we shall discuss further below.

Although we know little about the ISM relative abundances of the isomeric structures for the longer members of the series, our findings already provide a relevant result in the sense that, within the chemical route that we intend to explore in the present study, our data from Table 5 indicate that both isomers

would be important to investigate in order to consider both chemical paths to the formation of their corresponding anions. However, we shall mainly discuss the reactions with the HCN and HNC reagents, to show that these paths to forming  $CN^-$  are equally possible in the different environments of the ISM that we are analyzing.

### 3. The Shapes of the Reactive Surfaces

As discussed before, all reactions of interest in this study are strongly exothermic. Furthermore, our previous experience with such processes, as discussed in Gianturco et al. (2016) and Satta et al. (2015), has shown us that they are dominated by a collinear minimum energy path (MEP) and without any barrier existing between reagents and products. The suggested mechanism, in fact, is given in Gianturco et al. (2016) and Satta et al. (2015) as one in which the initial ET process occurs during the approach between the two hydrogen atoms: the H-C bond is stretched as the H anion is approaching, thereby allowing for the starting of the ET exothermic step, from the approaching  $H^-$  initially to the C-end of the molecular partner, and finally, and chiefly, to the N-end of the radicals ( $C_xN^-$ ). The formation of a TS configuration as the partners approach each other more closely leads to additional energy release into the final products by forming a neutral, vibrationally cold  $H_2$  molecule that separates from the highly stretched configuration it has within the transition complex. A pictorial representation of the 3D surface describing the reaction (RPES) is reported by Figure 1, where the two panels compare the two isomeric variants we have discussed before. The left panel therefore shows the reaction of  $H^-$  with HCN, while the one on the right reports the same reaction but with HNC: both sets of reagents yield  $H_2$  and  $CN^-$  as products.

It is evident from a perusal of both surfaces that the two reactions proceed in the same fashion: no energy barriers between reagents (on the left region of each RPES) and products (on the right region of the same surfaces) and a marked exothermicity, which, for the case of the HNC, is even larger by more than 0.5 eV (see data in Table 5). We therefore expect that both reactions can play a role in the ISM regions where both molecules in question have been observed.

It is also interesting to note here that both energy surfaces show an intermediate, smaller energy minimum at the stretched distances of the C-H end of the partner molecular chain (around 2–4 Å) and at even larger values of the H-H distances of about 4 Å. One could suggest that in that outer well region the initial ET step begins to occur while the molecular hydrogen is still strongly vibrationally excited and the terminal H atom has moved far away from the residual cyano derivative. In other words, the excess electron would initially “transfer” to the H-end of the chain and finally to the CN-end of the new anion after the  $H_2$  is formed as one of the molecular products. It is thus at the second energy minimum, which is now deeper and occurs at the shorter C-H/N-H distances at which the neutral,  $H_2$  molecule starts to get formed (second exothermic step) by releasing its vibrational energy content and thus reaching the variationally optimized TS, which evolves toward finally producing  $H_2$  in its vibrational ground state as it separates from the anionic product.

In the two panels of Figure 2 we further report the RPES shape for the reaction involving the next member of the cyanopolyne series: the  $HC_3N$  neutral partner of  $H^-$ . The foreground of the upper panel of the figure shows the  $H^-$

## Collinear approach

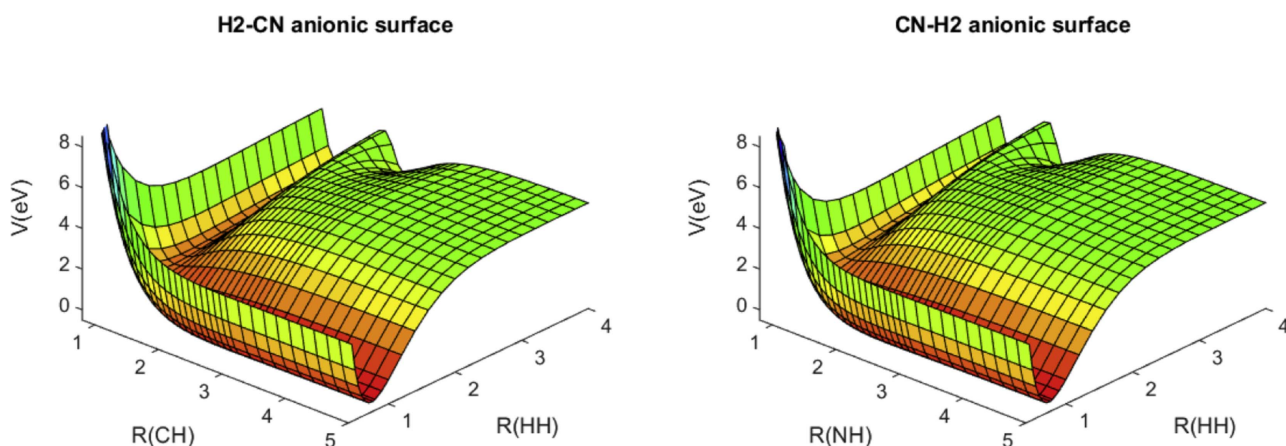


**Figure 1.** Computed reactive PES for the formation of  $\text{CN}^-$  from either  $\text{H}^- + \text{HCN}$  (left panel) or  $\text{H}^- + \text{HNC}$  (right panel). See the main text for further discussion.

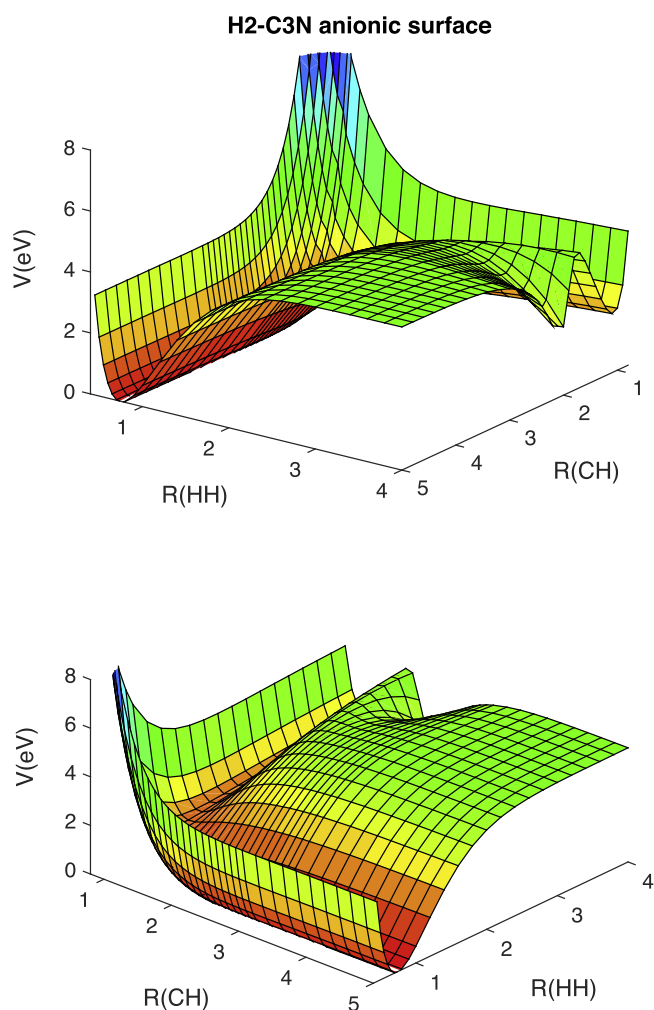


**Figure 2.** Two different views of the reactive PES for the  $\text{H}^- + \text{HC}_3\text{N}$  reaction. The upper panel shows the entrance channels on the upper right region of the RPES, while the lower panel reports the products' channel on the lower right portion of the surface. See the main text for further details.

approach to the  $\text{HC}_3\text{N}$  reagent (from right to left) and the clear exothermic, barrierless path down to  $\text{H}_2$  formation and  $\text{C}_3\text{N}^-$  separation is shown in the valley to skewing toward the left in

that panel. On the other hand, the rotated view presented in the lower panel indicates on the extreme left the incoming exothermic path for the  $\text{H}^-$  approach to the C–H end of  $\text{HC}_3\text{N}$ , followed by the further exothermic outgoing  $\text{C}_3\text{N}^-$  and the cold  $\text{H}_2$  formation along the valley shown in the foreground, from left to right.

From the upper view of the RPES shown in that Figure 2 we see even more clearly the role of the outer, shallower energy well that we associate with the initial ET step, while the H–H bond is still describing a highly vibrationally excited pair of H atoms, the external one also being far away from the residual cyano derivative fragment. It is thus an indication of the occurrence of a nonadiabatic curve-crossing effect that transfers the  $\text{H}^-$  charge to the terminal H atom of the cyanopolyne partner. It is then the deeper well located at the shorter C–H distances which will permit the exothermic release of that vibrational energy along the evolution of the variationally optimized TS complex (as we shall discuss in more detail in the next section) that can now decay into the final “cold” molecular products without any intermediate energy barrier and having completed the ET step to the final anionic product.

In conclusion, this member of the cyanopolyne series also shows its reaction with  $\text{H}^-$  to be a barrierless, exothermic process along a nearly collinear path. Along that path, in fact, one gains energy by the occurrence of an initial ET process that takes place for highly stretched C–H and H–H bonds between partners. The release of that vibrational energy in both bonds helps the TS formation at the bottom of the RPES, at the start of the MEP path. As we shall further explain in the next section, along such a reaction path the formation of a cold H–H neutral molecule, plus the outgoing anionic linear chain as one of the products, can now occur in a strong exothermic and barrierless fashion.

The same general features of this reaction are also observed along the collinear MEP energy evolution shown in Figure 3 for the next two members of the series,  $\text{C}_5\text{N}^-$  and  $\text{C}_7\text{N}^-$ .

In both instances the process remains, as before, strongly exothermic and without any barrier between reagents and products after the occurrence of the initial ET step indicated by the presence in both systems of the outer, shallower energy well for vibrationally excited C–H H–H distances. Once the

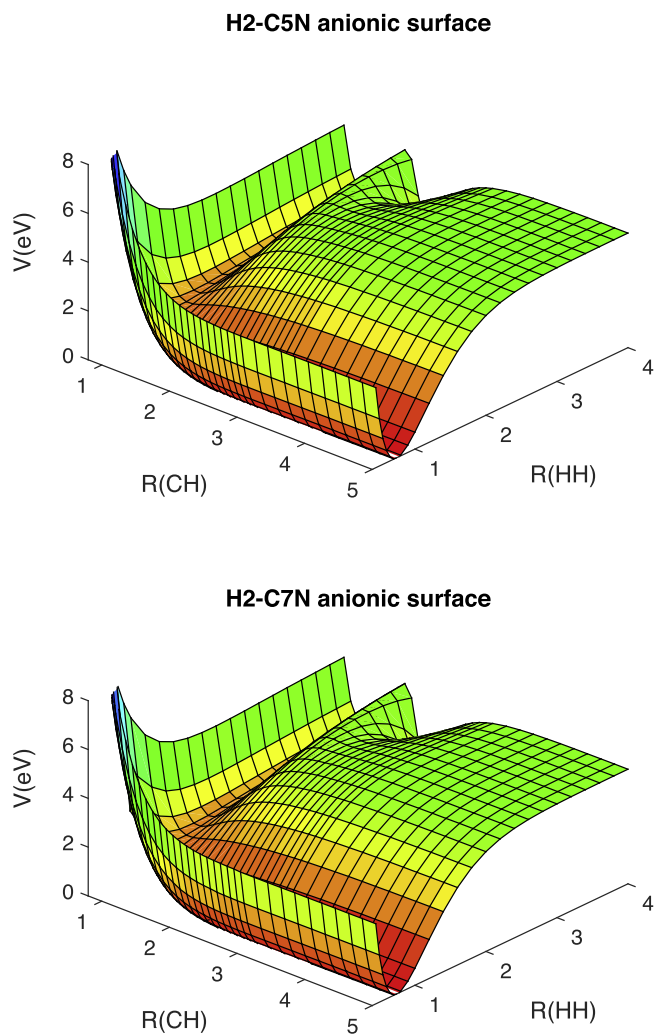


**Figure 3.** Computed 3D presentation for the collinear MEPs relative to the next larger members of the cyanopolyne series. Upper panel:  $\text{H}^- + \text{HC}_5\text{N}$ ; lower panel:  $\text{H}^- + \text{HC}_7\text{N}$ . See the main text for further details.

deeper well of the RPES is reached at shorter distances within the complex, the systems reach configurations where both the above bonds are shorter and close to their equilibrium values. This means that the reactions can now follow the exothermic MEP evolutions without any intermediate barrier, as we have already explained before.

Another interesting way of visualizing the exothermicity of the present reactions is shown by the two panels of Figure 4, where we choose as an example the isomer reactions involving HCN/HNC partners.

Both panels of Figure 4 present the collinear reaction paths after “cold”  $\text{H}_2$  formation has occurred and the initial vibrational energy of that bond has been released: the formed anion now recedes from the complex region. The H–H distance is also that of the optimized complex geometry in both cases (see the next section’s discussion). The upper panel clearly shows that in both reactions the formed anions leave the complex along a monotonically decreasing path, since the formation of a vibrationally cold, neutral  $\text{H}_2$  now affords the systems the chance to undergo a substantial energy release without any intermediate barrier.

In that same figure, we have enlarged the energy region, where either the H–C or the H–N distances are clearly down,

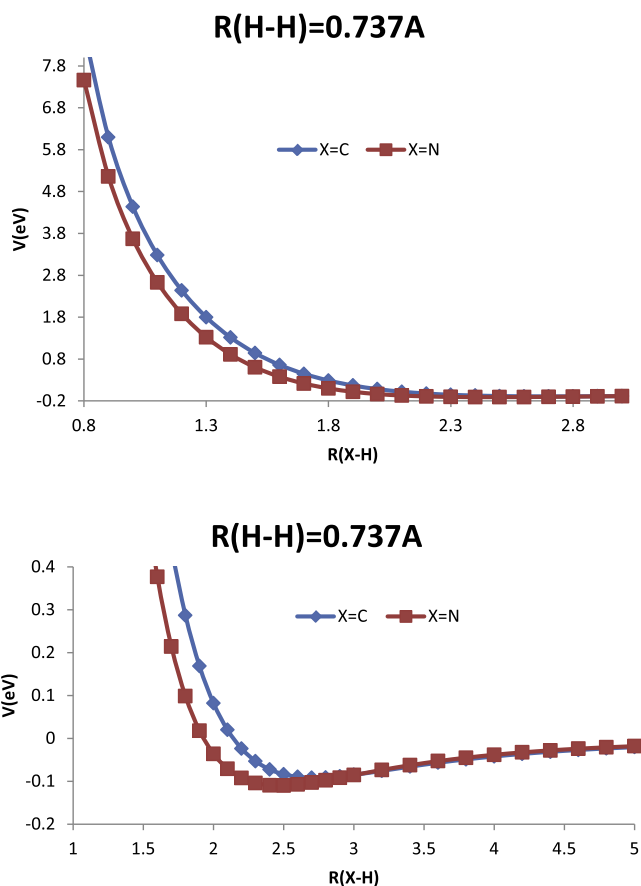


**Figure 4.** Different collinear “cuts” for the reaction of  $\text{H}^- + \text{HCN}$ , given by small lozenges, and  $\text{H}^- + \text{HNC}$ , given by large squares, at fixed H–H distances for the geometry of the complex. The “X” symbols denote the remaining chains from either end of approach for the  $\text{H}^-$  partner. See the main text for further details.

into a flat outgoing path. It now shows in both cases the presence of a very shallow well indicating the absolute minimum energy location of the complex configurations before the final release of the two products, as mentioned already when analyzing the previous figures. Although the reaction with HNC shows a slightly larger well ( $-0.11$  eV versus  $-0.09$  eV) into their configurations of the reaction complex, both systems can easily make out to products even at the lower temperatures, due to the marked shallowness of such small minimum regions. However, this can energetically happen, provided the initial ET step has been allowed to occur along the outer wells shown by Figure 2 and already discussed earlier in this section.

In the next section we will use the present RPES of the collinear approaches to help us to obtain the corresponding reaction rates over a broad range of temperatures, following the nonlinear, 3D model of the Variational Transition State Theory (VTST).

#### 4. Modeling the Reaction Rates

We have seen in the previous discussion that all the reactions evolve on RPESs that are markedly exothermic and present no energy barriers along the MEP evolutions from reagents to products. Furthermore, the calculations of the relative energetics between reagents and products, for all the members of the series we have examined, indicate a marked increase of

exothermicity in going from one set of  $\text{HC}_x\text{N}$  partner to the  $\text{HNC}_x$  isomeric variants. This last feature will be discussed below, as an example, for the case of  $\text{HCN}/\text{HNC}$  systems.

The special features of the reaction energetics have allowed us to use a version of the Rice–Ramsperger–Kassel–Marcus (RRKM) approach based on the VTST treatment for obtaining temperature-dependent rates, as discussed in Fernandez-Ramos et al. (2006) for the case of exothermic, barrierless reactions. This approach is basically assuming that, for the present types of reactions, the formation of a transition state complex along the exothermic energy path from reactants to products controls the efficiency of product formation via the relative energetics between the partition functions (PFs) of that complex and those of the final products.

In particular, within the RRKM approach for the description of a TS configuration, one assumes a strong-coupling approximation whereby the degrees of freedom within the TS complex are strongly coupled among themselves and therefore the entire available phase-space will be occupied by the PFs associated with the TS on a shorter timescale than that of the characteristic reaction time step: see Fernandez-Ramos et al. (2006). This means that, once the TS complex is reached by the reagents along the exothermic MEPs, the reactants are in microcanonical equilibrium. The TS complex PF,  $Q_{\text{TS}}^\ddagger$ , can then be obtained as the product of the PFs for the conserved mode PFs within that complex,  $Q_{\text{cons}}^\ddagger$ , times the PFs of the translational modes, which are evolving along the MEP following the complex geometry,  $Q_{\text{trans}}^\ddagger$ . The latter modes now make the complex evolve from reagents to products, thereby acting as the active modes of the reaction:

$$Q_{\text{TS}}^\ddagger(T) = Q_{\text{cons}}^\ddagger(T)Q_{\text{trans}}^\ddagger(T). \quad (4)$$

In our case, the translational modes for the title reactions will be those indicated in the 3D energy maps of the previous section: the  $\text{H}^- \cdots \text{H}$  distance and the  $\text{H} \cdots \text{C}$  distance along the collinear path. We shall see later that such a simpler approach holds well for the  $x = 1$  case, while the larger chains will require a multidimensional optimization along the increasingly nonlinear TS structures formed along their respective MEPs. The pre-exponential factor of the reaction rate formulations now becomes the only significant part that needs evaluation in order to obtain the required reaction rates  $K(T)$ . Thus, the latter quantities can now be obtained as the ratios between the relevant PFs of the TS complex and those of the reagents, as a function of the reaction temperatures:

$$K(T) = \frac{k_B T}{h} \frac{Q^\ddagger[\text{H}^- - \text{HC}_x\text{N}]}{Q[\text{HC}_x\text{N}]Q[\text{H}^-]}. \quad (5)$$

Here,  $k_B$  is the Boltzmann constant and  $h$  is the Planck's constant. The PFs of the reaction complex are variationally minimized along all the optimized geometries of the MEP. After the variational minimization we therefore obtain at each temperature the TS geometries at the lowest possible energy along the MEP paths and within the VTST model; see Fernandez-Ramos et al. (2006).

Note that the rate coefficient as obtained from (5) is mainly controlled, at the lowest temperatures, by the behavior of the vibrational part of the PF for that specific TS geometry, since all other degrees of freedom are now “frozen” to their lowest values. In turn, such low-temperature PFs relate directly to the zero-point energy (ZPE) values of the modes under consideration since  $Q_{\text{vib}}$  (at low T) can be written as  $\propto e^{-E_{\text{ZPE}}/KT}$ . Thus,

**Table 6**  
Computed Structures of the TS over a Broad Range of Temperature for the Smaller Members of the Present Cyanopolyne Chains

HCN					
$T$	HH	HC			
10–340	1.721	1.055			
345–475	1.712	1.059			
480–500	1.702	1.062			
HC <sub>3</sub> N					
$T$	HH	HC <sub>1</sub>	HHC <sub>1</sub>	HC <sub>1</sub> C <sub>2</sub>	C <sub>1</sub> C <sub>2</sub> C <sub>3</sub>
10–255	1.713	1.030	158.12	166.31	179.04
260–350	1.702	1.034	158.38	166.00	179.01
355–440	1.692	1.037	158.64	165.69	178.98
445–500	1.681	1.041	158.88	165.37	178.95

**Note.** Distances in Å, angle in degrees.

the overall rates at low- $T$  would be linked with the features of the corresponding ZPE energy values within the PFs:

$$K(\text{low}T) \propto T^2 \exp \frac{-E_{\text{ZPE}}^{\text{TS}} + E_{\text{ZPE}}^{\text{Reactants}}}{k_B T} \propto T^2 \exp \frac{-\Delta_{\text{ZPE}}}{k_B T}; \quad (6)$$

in the present reactions we have that the  $E_{\text{ZPE}}^{\text{reactants}} = E_{\text{ZPE}}^{\text{HC}_x\text{N}}$ , since  $\text{H}^-$  does not contribute to it. The quantity  $\Delta_{\text{ZPE}}$  thus defines the energy differences between the ZPEs of the reactants and those of the TS complex. It therefore controls the slope of the reaction rate  $K(\text{low}T)$ , which is defined by the above equation: a large value for that difference causes a greater decrease of  $K(T)$  as  $T$  decreases. The  $\Delta_{\text{ZPE}}$  values of our present MEPs depend on: (i) the H–C vibrations at the TS geometries and (ii) the intramolecular vibrational frequencies within the remaining chain of atoms in the reactants. Since we found that the TS has a linear geometry for  $x = 1$ , but it has increasingly more bent structures for  $x$  increasing from 3, to 5, to 7 (see Tables 6 and 7 below), then the  $\Delta_{\text{ZPE}}$  is the largest for the HCN member of the series, while it becomes increasingly smaller for increasingly larger members of the present series. We report in detail in Tables 6 and 7 all the geometric parameters for the TS structures we have found for our VTST calculations. We should note here that the calculations for  $x = 1$  and  $x = 3$  had been carried out already in our earlier work on the present mechanism (Satta et al. 2015), where we employed a smaller basis set expansion for the RPES calculations and carried out the VTST calculations over a less dense grid of points. The present improved results, however, remain within less than 5% of the earlier ones and exhibit exactly the same temperature dependence.

The data of these tables show, from the top to the bottom panels, the  $x = 1$  to  $x = 7$  cases. The first two columns report the distances of the atoms in the complex, the H–H and H–C<sub>1</sub>, while the next columns give angles along the bent structures of the longer members of the series. Only the H–HCN reaction shows a linear TS structure.

Since, within the RRKM approach which we have used in the present modeling, the structure of the TS is crucially linked to the expression for the resulting rate coefficient via Equations (5) and (6), note the following from a perusal of the data reported in the above tables.

**Table 7**

Computed Structures of the TS over a Broad Range of Temperature for the Larger Members of the Present Cyanopolyne Chains

HC <sub>5</sub> N						
<i>T</i>	HH	HC <sub>1</sub>	HHC <sub>1</sub>	HC <sub>1</sub> C <sub>2</sub>	C <sub>1</sub> C <sub>2</sub> C <sub>3</sub>	C <sub>2</sub> C <sub>3</sub> C <sub>4</sub>
10–70	1.537	1.056	151.65	156.27	177.22	178.90
75–130	1.524	1.060	152.10	155.74	177.17	178.90
135–190	1.510	1.064	152.53	155.19	177.12	178.90
195–240	1.497	1.067	152.95	154.64	177.07	178.91
245–295	1.483	1.071	153.36	154.09	177.03	178.91
300–350	1.470	1.075	153.75	153.53	176.99	178.91
355–410	1.456	1.079	154.12	152.97	176.95	178.91
415–480	1.442	1.082	154.49	152.41	176.91	178.91
485–500	1.429	1.086	154.84	151.84	176.88	178.91
HC <sub>7</sub> N						
<i>T</i>	HH	HC <sub>1</sub>	HHC <sub>1</sub>	HC <sub>1</sub> C <sub>2</sub>	C <sub>1</sub> C <sub>2</sub> C <sub>3</sub>	C <sub>2</sub> C <sub>3</sub> C <sub>4</sub>
10–35	1.476	1.062	148.39	153.34	176.52	178.64
40–75	1.462	1.066	148.96	152.69	176.46	178.64
80–115	1.447	1.070	149.51	151.04	176.40	178.65
120–165	1.433	1.074	150.04	151.40	176.35	178.65
170–210	1.418	1.077	150.55	150.76	176.30	178.65
215–270	1.404	1.081	151.03	150.12	176.26	178.66
275–315	1.389	1.085	151.50	149.47	176.22	178.66
320–365	1.375	1.089	151.95	148.84	176.19	178.66
370–420	1.361	1.092	152.37	148.21	176.17	178.67
425–465	1.347	1.096	152.79	147.58	176.14	178.67
470–500	1.333	1.100	153.19	146.96	176.13	178.67

**Note.** Distances in Å, angle in degrees.

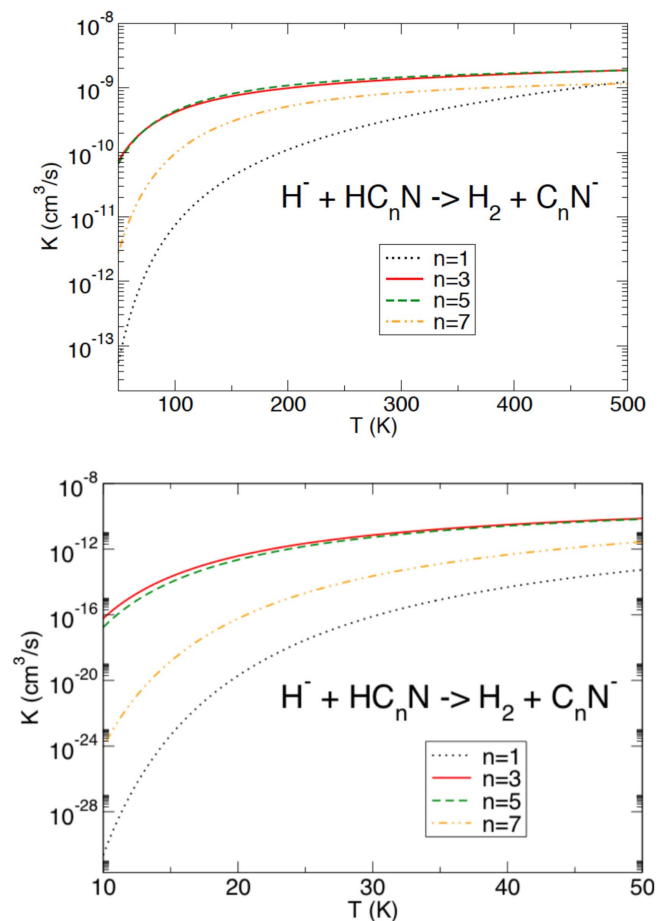
- (i) The structures of the TSs change little over a very broad range of temperatures, indicating that the variational determination of the TS is correctly obtained: along an exothermic, barrierless path the structure of the final complex should change little from its minimum structure.
- (ii) As the length of the chain increases we see more marked departures from linearity along what we have defined as the “translational” coordinates, which are active along the MEP and which involve the X–C–H–H bonds, while the C-atoms further away seem to maintain a nearly linear structure. This means that only the nearest triple bond is affected by the polarization changes during the ET process, while those further away along the chain remain largely unchanged, as expected.
- (iii) The modification of that triple bond, on the occurrence of excess charge initial transfer, which reaches its final, main localization at the terminal N atom of the product anion, also affects the  $\Delta_{ZPE}$  energy gaps discussed before, a feature which is crucial for the low-*T* behavior of the rate coefficients (see Equation (6)); it then follows that the  $\Delta_{ZPE}$  value increases again from  $x = 3$  to  $x = 5$  and  $x = 7$ . This feature will be further discussed in our analysis of the low-temperature behavior of the present rates.

We have fitted all the computed rates following the standard formula suggested earlier for such systems (see Gianturco et al. 2016; Satta et al. 2015; and Prasad & Huntress 1980) and we therefore report the actual fitting parameters in Table 8 for the higher-*T* range (upper panel) and the low-*T* range (lower panel). The actual fitting formula is also reported at the bottom of that table.

**Table 8**Fitting Parameters for the Rate Coefficients Computed in the Present Work, Given for the High-*T* Range (Upper Panel) and the Low-*T* Range (Lower Panel)

<i>T</i> (K)	<i>n</i>	$\alpha$ (cm <sup>3</sup> s <sup>-1</sup> )	$\beta$	$\gamma$ (K)
100–500	1	9.0368e-10	1.7361	284.429
	3	2.3052e-9	1.7589e-1	153.699
	5	2.7539e-9	-3.7352e-2	188.310
	7	3.1121e-9	-3.9163e-1	391.083
10–100	1	1.8152e-9	6.4397e-1	479.034
	3	2.4787e-9	4.9065e-2	173.248
	5	2.7820e-9	-4.9593e-2	190.971
	7	2.8484e-9	-2.4470e-1	367.335

$$K(T) = \alpha \left( \frac{T}{300} \right)^\beta e^{-\frac{\gamma}{T}}$$

**Note.** The actual fitting formula is given at the bottom of the table.**Figure 5.** Computed temperature dependence of the reaction rates of the present study from CN<sup>-</sup> to C<sub>7</sub>N<sup>-</sup> for the odd values of the *x* index. The lower panel reports the low-*T* behavior, while the upper panel gives the higher-*T* behavior of the rates of formation.

The data for the  $x = 1$  member of the series will be discussed later in comparison with the HNC isomeric variant.

The temperature behavior of the computed rates is reported for all present systems by the two panels of Figure 5.

The following comments can be made by observing the rate behavior in that figure.

- (i) As expected, the formation of CN<sup>-</sup> remains the least efficient chemical process in reaction with H<sup>-</sup>. All other

**Table 9**

Computed Rate Values, at Four Different Temperatures, for the Present Series of Cyanopolyynes (in Units of  $\text{cm}^3 \text{mol}^{-1} \text{s}^{-1}$ )

$n$	10 K	30 K	50 K	100 K
1	2.29(−31)	7.85(−17)	5.53(−14)	7.40(−12)
3	5.96(−17)	7.10(−12)	7.34(−11)	4.19(−10)
5	1.71(−17)	5.29(−12)	6.67(−11)	4.38(−10)
7	8.58(−25)	2.26(−14)	2.75(−12)	9.57(−11)

members of the series exhibit larger reaction rates at all temperatures. As discussed earlier, this feature has to do with the instability of the anion of the molecular reaction partner and therefore with the importance of initiating the ET step only at large bond distances for the H–CN fragment of the reacting cyanopolyyne, where the final hydrogen molecule has not yet been formed. At low temperatures that step may not occur, while at higher temperatures its increased occurrence is still limited by the fewer degrees of freedom of the PF of its transition complex.

- (ii) The largest rates are seen to occur for the formation of  $\text{C}_3\text{N}^-$ , and close to it in size, by the formation of  $\text{C}_5\text{N}^-$ . These are the two species exhibiting the largest rates of formation from the present calculations. Since both systems were shown to have TS complexes not far from the more efficient linear structures, it stands to reason that both molecular anions are formed with larger rates with respect to those of the  $x = 1$  system, where the reduced number of degrees of freedom involved in its PFs limits the size of the corresponding rates.
- (iii) The largest member of the series,  $\text{C}_7\text{N}^-$  shows a smaller rate of formation at all T, smaller than the  $x = 3$  and 5 members but still larger than the  $x = 1$  member. This difference has to do with the fact that, as discussed earlier, the TS variationally optimized structures are now far from the linear configurations and therefore the bending of the longer chain attached to the active coordinates reduces the numerator in (5), which in turn lowers the value of the associated reaction rate. Furthermore, note that, with the exclusion for the moment of the  $x = 1$  member, the  $x = 3$  and 5 anions are seen in our calculations to be associated with the largest rates of reaction. They are two members of the present series of molecules for which the anions have been repeatedly detected in the ISM, while  $\text{C}_7\text{N}^-$ 's larger member, so far, has not yet been detected by observational studies (e.g., see Millar et al. (2017)).
- (iv) One should also note that the Langevin rates listed in the KIDA database of Wakelam et al. (2012) for  $\text{CN}^-$  are about  $3.8 \cdot 10^{-9} \text{cm}^3 \text{mol}^{-1} \text{s}^{-1}$  and are independent of temperature. They are obviously always overestimating all present rates and at all temperatures.

Another interesting set of comparisons between the values of the rates of formation, at four selected temperatures indicative of different regions of the ISM, is reported in Table 9 for the four members of the cyanopolyyne series of this work.

One can see that at the lowest shown temperature of 10 K the formations of  $\text{CN}^-$  and  $\text{C}_7\text{N}^-$  are really negligible, while the formations of  $\text{C}_3\text{N}^-$  and  $\text{C}_5\text{N}^-$  are still small but many orders of magnitude larger. The effects are more marked for the region between 30 and 100 K, indicatively corresponding to the

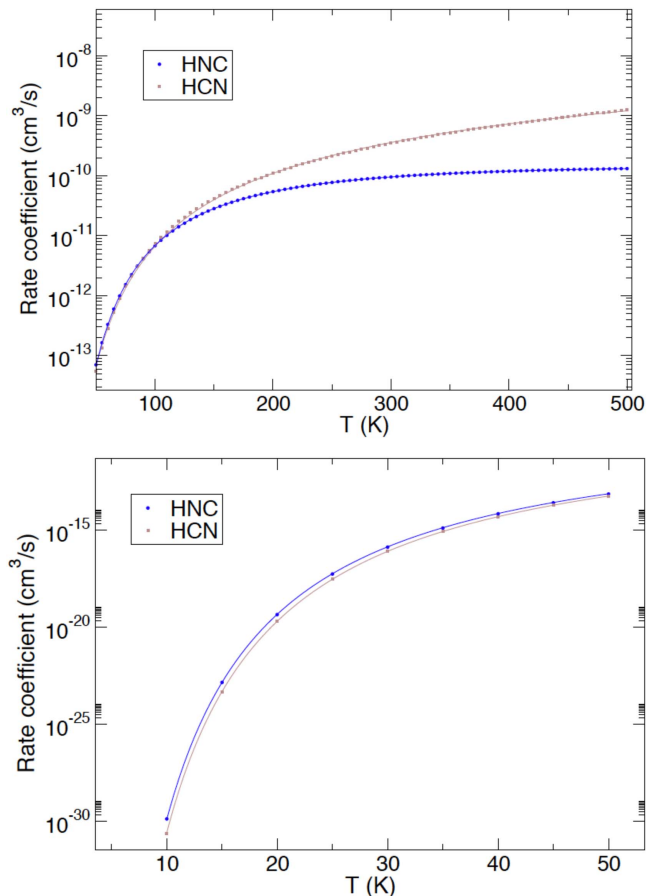


**Figure 6.** Computed formation rates of  $\text{CN}^-$  from both isomeric forms of the initial reagent, HCN and HNC. See the main text for further details. Lower panel: low- $T$  range; upper panel: high- $T$  range.

averaged temperatures of dark molecular clouds and CSE environments; see Millar et al. (2017). In these intervals we see that the rates of formation become much larger for all four systems, albeit still being largest for  $\text{C}_3\text{N}^-$  and  $\text{C}_5\text{N}^-$ . Such data indicate that the possibility of forming all anions by chemical routes becomes significant for the latter molecules and is in clear competition with REA processes that have been shown as having much smaller rates of formation associated with them. One should also be reminded that for temperatures around 50 K, the chemical rates of formation of the  $x = 1$  member of the present series are already orders of magnitude larger than their calculated REA rates around 100 K (see Khamesian et al. 2016). It therefore follows that even for the smallest member of the present series of anions, the chemical paths reported here are much more significant than the REA mechanism for explaining the formation of its anion.

Another interesting comparison between some of our data is shown in the panels of Figure 6, where the rates of formation of  $\text{CN}^-$  are shown for both the isomer partners of  $\text{H}^-$ , HCN and HNC.

Note that both reagents, as expected, behave very similarly as a function of temperature. The low- $T$  formation rates are very close to each other, although the  $\text{CN}^-$  formation rate from HNC always remains slightly larger. As the temperature moves above 150 K we see that the differences in size increase and the trend is inverted. We see in the upper panel of Figure 6 that the HNC reagent yields formation rates that are increasingly smaller, reaching nearly one order of magnitude smaller around

**Table 10**  
Computed Fitting Parameters for the T-dependence of the Formation Rates of  $\text{CN}^-$  from HNC (left) and HCN (right)  
(the Formula is the Same as Those of Tables 6 and 7)

	HNC		HCN	
$T$ (K)	10–50	50–500	10–50	50–500
$\alpha$ ( $\text{cm}^3 \text{s}^{-1}$ )	$4.9394 \cdot 10^{-10}$	$5.2509 \cdot 10^{-10}$	$6.9512 \cdot 10^{-10}$	$1.1986 \cdot 10^{-9}$
$\beta$	–0.6029	–0.7082	–0.3966	1.4335
$\gamma$ (K)	495.3	511.6	507.5	362.1

**Note.** All rates are in units of  $\text{cm}^3 \text{mol}^{-1} \text{s}^{-1}$ .

500 K. On the whole, however, the rates of formation at 200 K and above remain of the order of  $10^{-10} \text{cm}^3 \text{mol}^{-1} \text{s}^{-1}$ , i.e., substantially larger than the corresponding rates of REA formation by electron attachment in Herbst & Osamura (2009), Kawaguchi et al. (1995), and Khamesian et al. (2016). All reaction rates, however, remain smaller than the Langevin formation rates usually employed in astrochemical databases, and which are, as mentioned earlier, of the order of  $10^{-9} \text{cm}^3 \text{mol}^{-1} \text{s}^{-1}$ , as given by Wakelam et al. (2012).

We summarize in Table 10 the fitting parameters for the two isomeric partners of the smallest members of the present series of cyanoderivatives, both leading to the formation of  $\text{CN}^-$ .

Note some possible reasons for the difference in the temperature dependence of the two rates. We already know that the HC bond is less strong than the HN bond in its isomeric variant, as shown by our data discussed in Section 2. We have already discussed before that, that at low- $T$ , the present chemical rates are controlled by the differences in ZPE values between the two TS (linear) for both molecules. Since the one for HCN is larger than for HNC, then the low- $T$  formation rates given by our VTS theory slightly favor the formation from HCN more than that from HNC. As the temperature increases, however, the contributions from the CN frequencies in HCN versus HNC are higher in the former with respect to the latter. Furthermore, the opposite occurs for the HC frequency in the TS with respect to the HN frequency: it is about  $3311 \text{cm}^{-1}$  in the former and  $3643 \text{cm}^{-1}$  in the latter. Thus, as the temperature increases, the stronger HN bond within the TS complex slows down the rate increase for HNC versus those for HCN. On the whole, however, both molecules can contribute to  $\text{CN}^-$  formation with similar rates, thereby making its probability of occurrence even larger than that via the REA route (about  $10^{-17} \text{cm}^3 \text{mol}^{-1} \text{s}^{-1}$  around 100 K: Herbst & Osamura 2009; Khamesian et al. 2016).

## 5. Present Conclusions

In the present work we have analyzed in detail the chemical formation of  $\text{C}_x\text{N}^-$  anionic species from a reaction with  $\text{H}^-$  of the corresponding cyanopolyne species:  $\text{HC}_x\text{N}$ , with  $x$  from 1 to 7. The aim has been to evaluate, for temperatures of significance under ISM conditions, the relative probabilities of forming the anions, and to show that this specific chemical route is likely to be more significant than the more popular electron attachment processes followed by radiative emission, which have long been considered for the chief source of those anions, i.e., the REA formation mechanism already discussed many times in the literature (see Herbst & Osamura 2009; Mackay et al. 1977; Carelli et al. 2014, 2013; and Khamesian et al. 2016).

We have carried out structural calculations for the reagents with  $x = 1, 3, 5, 7$  and further employed accurate ab initio

findings to generate the RPES along the collinear path. We have further calculated the nonlinear MEP to product formation. The behavior of all the above structural quantities along the series of cyanopolyynes has been discussed in detail in Sections 2 and 3.

In Section 4 we employed the computed MEP to obtain the anion formation rates of reaction using the VTS theory and examining the effects of nonlinear TS for the longer chains of the series. We thus found that while  $\text{CN}^-$  is formed via a linear MEP for the final RRKM TS that in turns decays into products, the longer chains with  $x = 3, 5$ , and 7 show an increasing importance of nonlinear TS structures for the formation of the complexes, a feature that finally produces a strongly bent transition complex for the  $x = 7$  member of the series, and corresponding rates of formation that are lower than those of the two preceding, smaller terms of the same series.

The calculations of the reaction rates also show a distinct behavior as a function of temperature: (i) a very rapid increase of several orders of magnitude when going from a few K to about 100 K, and (ii) a smoother increase with temperature when  $T$  increases up to 500–1000 K. This behavior was shown here to be linked to the importance of the ZPE differences between reactants and their TS structures. In fact, we found them to be smallest for the  $\text{C}_3\text{N}^-$  formation reaction, so that the latter rates show the largest values in the low- $T$  regimes.

All reactions were found to be strongly exothermic, without a barrier from reactants to products and forming a TS complex along the MEP. It is along that path that the reactants undergo  $\text{H}_2$  formation in its lowest vibrational state, following an ET process that begins to take place when forming an initial complex with a highly stretched H–H reagent and finally evolves to the anionic  $\text{C}_x\text{N}^-$  product. The computed rate values reported by Table 9 show that in going from 10 to 100 K they change differently for each member of the series: the least reactive HCN changes nearly 20 orders of magnitude, while the more efficient formations of  $\text{C}_3\text{N}^-$  and  $\text{C}_5\text{N}^-$  vary by about 7 orders of magnitude: the changes with temperature therefore turn out to be very dramatic, for reasons explained in the previous section.

In the range of temperatures likely to be present in CSE environments, where those anions have been detected (e.g., see the review by Millar et al. 2017), we therefore see that the present chemical process for  $\text{C}_3\text{N}^-$  is several orders of magnitude larger than the REA rate of formation (Mackay et al. 1977; Khamesian et al. 2016).

Furthermore, we also see that the size of the Langevin rates of anion formation, usually employed in modeling studies (see, e.g., Wakelam et al. 2012), are invariably larger than any of our computed rates. This indicates the low reliability of using such estimates for the present ionic reactions.

Another interesting result from the present calculations is the analysis of the rates of formation for the HCN/HNC isomers. Their relative abundances in the ISM have been discovered to be very different from the one on earth, thus suggesting that both species could contribute equally to the production of  $\text{CN}^-$  anions. In fact, our calculations for both species, presented in Figure 6, indicate their rates to exhibit some differences as a function of temperature, but to be essentially of the same order of magnitude, around 100–200 K. Given the fact that the REA path of formation was found to be several orders of magnitude smaller over the same range of temperature (Khamesian et al. 2016), our findings suggest again that the present chemical route to  $\text{CN}^-$  formation is a more efficient mechanism for forming that anion in the CSE environments or dark molecular clouds.

The present calculations further indicate that the  $x = 7$  case produces RRKM rates of formation that are smaller than those of the shorter chains with  $x = 3$  and 5, this being more so in the lower- $T$  range below 50 K. The specific structural reason provided by our calculations indicates that the TS complex along the MEP for this reaction strongly favor bent structures, which therefore increases the importance of bending vibrations within the PF of the complex. This results in a reduction of the rate values obtained within the VTST model.

Such a finding is in line with the fact that, thus far, the  $\text{C}_7\text{N}^-$  anionic molecule has not been observed, although  $\text{HC}_7\text{N}$  has been observed (Millar et al. 2017). On the other hand, both  $\text{C}_3\text{N}^-$  and  $\text{C}_5\text{N}^-$  have been detected by Gupta et al. (2007) and Herbst (1981).

The following conclusions can therefore be drawn from the results of the present calculations.

- (i) The chemical paths to anionic derivatives from initially neutral cyanopolyyne in reaction with  $\text{H}^-$  are shown to be more effective than the REA paths (whenever available) at the ISM temperature of interest.
- (ii) The  $\text{C}_3\text{N}^-$  and  $\text{C}_5\text{N}^-$  formations exhibit the largest chemical rates in the range of 50–100 K and therefore the present reactions are shown to be very effective mechanisms for their formation.
- (iii) The formation of  $\text{CN}^-$  can occur via two different reagents, HCN and HNC, which were shown to have very similar rates. Albeit the smallest rates found by our calculations, their combined occurrence can be markedly larger than the existing REA rates indicated in the current literature (Khamesian et al. 2016), thereby making this chemical reaction an important path to their formation.
- (iv) The  $\text{C}_7\text{N}^-$  formation rates turn out to be smaller than the presiding shorter members of the series, thus suggesting this chemical “inefficiency” as a possible cause for the lack of its observational detection as discussed in Millar et al. (2017).

The present chemical study therefore confirms from ab initio calculations that the analysis of ion–molecule reactions involving  $\text{H}^-$  should be experimentally attempted with cyanopolyyne to search for chemical routes to the formation of anionic (C, N)-containing linear chains like those observed

already found in different ISM environments (Millar et al. 2017).

F.A.G. and R.W. thank the Austrian Science Fund (FWF) for supporting the present research through project P27047-N20.

## ORCID iDs

F. A. Gianturco  <https://orcid.org/0000-0003-3962-530X>

R. Wester  <https://orcid.org/0000-0001-7935-6066>

## References

- Baccarelli, I., Sebastianelli, F., Nestmann, B., & Gianturco, F. A. 2013, *EPJD*, **67**, 93
- Botschwina, P., & Oswald, R. 2008, *JChPh*, **129**, 044305
- Brunken, S., Gupta, H., Gottlieb, C. A., Mc Carthy, M. C., & Thaddeus, P. 2007, *ApJL*, **664**, L43
- Carelli, F., Gianturco, F. A., Wester, R., & Satta, S. M. 2014, *JChPh*, **141**, 054302
- Carelli, F., Satta, M., Grassi, T., & Gianturco, F. A. 2013, *ApJ*, **774**, 97
- Cernicharo, J., Guelin, M., Agundez, M., et al. 2007, *A&A*, **467**, L37
- Dalgarno, R. A. 1973, *ApJ*, **181**, 95
- Douguet, N., Fonseca dos Santos, S., Rault, M., et al. 2013, *PhRvA*, **88**, 052710
- Fernandez-Ramos, A., Miller, J. A., Klippenstein, S. J., & Truhlar, D. G. 2006, *ChRv*, **106**, 4518
- Fortenberry, R. C., & Crawford, D. T. 2011, *JChPh*, **134**, 154304
- Gao, Y., & Solomon, P. M. 2004, *ApJS*, **152**, 63
- Gianturco, F. A., Satta, M., Mendolicchio, M., et al. 2016, *ApJ*, **830**, 2
- Graninger, D., Oberg, K., Qi, C., & Kostner, J. 2015, *ApJL*, **807**, L15
- Gupta, H., Brunken, F., Tainassia, S., et al. 2007, *ApJL*, **655**, L57
- Herbst, E. 1981, *Natur*, **289**, 656
- Herbst, E., & Osamura, Y. 2009, *ApJ*, **679**, 1670
- Herbst, E., & Woon, D. E. 1997, *ApJ*, **489**, 109
- Hogerheijde, M. R., Jansen, D. J., & van Dishoeck, E. F. 1995, *A&A*, **294**, 792
- Jin, M., Lee, J. E., & Kim, K. T. 2015, *ApJS*, **219**, 2
- Kawaguchi, K., Kasai, Y., Ishikawa, S., & Kaifu, N. 1995, *PASJ*, **47**, 853
- Khamesian, M., Douguet, N., Fonseca dos Santos, S., et al. 2016, *PhRvL*, **117**, 123001
- Kolos, R., Gronowski, M., & Botschwina, P. 2008, *JChPh*, **128**, 154305
- Lis, D. D., Backelee-Morvan, D., Boissier, J., Crovisier, J., Biver, N., & Charnley, S. B. 2008, *ApJ*, **675**, 931
- Listz, H., & Lucas, R. 2001, *A&A*, **370**, 576
- Mackay, G. I., Tanaka, K., & Bohme, D. K. 1977, *IJMP*, **24**, 125
- McCarthy, M. C., Gottlieb, C. A., Gupta, H., & Thaddeus, P. 2006, *ApJL*, **652**, L141
- Millar, T. J., Walsh, C., & Field, T. A. 2017, *ChRv*, **117**, 1765
- Mily-Blant, P., Walmsley, M., Pineu-des Forets, G., & Flower, D. 2010, *A&A*, **512**, A41
- Moreno, R., Lelouch, E., Lara, L. M., et al. 2011, *A&A*, **536**, L12
- Morisawa, Y., Hoshina, H., Kato, Y., et al. 2005, *PASJ*, **57**, 325
- Prasad, S. S., & Huntress, T. J., Jr. 1980, *ApJS*, **43**, 1
- Remijan, A. J., Hollis, J. M., Lovas, F. J., et al. 2007, *ApJL*, **664**, L47
- Sarrasin, E., Abdallah, D. B., Wernli, M., et al. 2010, *MNRAS*, **404**, 518
- Sarre, P. J. 1980, *JChPh*, **77**, 769
- Satta, M., Gianturco, F. A., Carelli, F., & Wester, R. 2015, *ApJ*, **799**, 228
- Sebastianelli, F., & Gianturco, F. A. 2010, *EPJD*, **59**, 389
- Sebastianelli, F., & Gianturco, F. A. 2012, *EPJD*, **66**, 41
- Shiell, R. C., Hy, X. K., Hu, Q. C. J., & Hepburn, J. W. 2000, *Far. Disc. Chem. Soc.*, **115**, 331
- Thaddeus, P., Gottlieb, C. A., Gupta, H., et al. 2008, *ApJ*, **677**, 1132
- Thomson, R., & Dalby, F. W. 1968, *CaJPh*, **46**, 2815
- Turner, B. E., Pirogov, L., & Minh, Y. C. 1997, *ApJ*, **483**, 235
- Wakelam, O., et al. 2012, <http://kida.obs.u-boreaux1.fr>
- Werner, J.-H., Knowles, P. J., Knizia, G., et al. 2006, MOLPRO version 2006.1 a package of ab initio programs, <http://www.molpro.net>